
Enhancing Photocatalytic Performance of ZnO Nanoparticles Through Er/Al Co-Doping for Solar-Driven Environmental Remediation

[Raúl Bahamonde Soria](#)*, [Jefferson Estupiñan](#), [Irma Gonza](#), [Montserrat Naranjo](#), [Billy Daniel Chinchin](#), [Lucía E. Manangón](#), [Katherine Vaca](#), [Martha Romero-Bastidas](#), Henry Pupiales, [Verónica Taco](#), [Patricia Luis](#)

Posted Date: 7 July 2025

doi: 10.20944/preprints202507.0559.v1

Keywords: photocatalysis; ZnO nanoparticles; erbium; aluminum; sol-gel; anti-bacterial properties



Preprints.org is a free multidisciplinary platform providing preprint service that is dedicated to making early versions of research outputs permanently available and citable. Preprints posted at Preprints.org appear in Web of Science, Crossref, Google Scholar, Scilit, Europe PMC.

Copyright: This open access article is published under a Creative Commons CC BY 4.0 license, which permit the free download, distribution, and reuse, provided that the author and preprint are cited in any reuse.

Disclaimer/Publisher's Note: The statements, opinions, and data contained in all publications are solely those of the individual author(s) and contributor(s) and not of MDPI and/or the editor(s). MDPI and/or the editor(s) disclaim responsibility for any injury to people or property resulting from any ideas, methods, instructions, or products referred to in the content.

Article

Enhancing Photocatalytic Performance of ZnO Nanoparticles Through Er/Al Co-Doping for Solar-Driven Environmental Remediation

Raúl Bahamonde Soria ^{1,2,*}, Jefferson Estupiñan ^{1,3}, Irma Gonza ^{1,4}, Monserrat Naranjo ¹, Billy Chinchin ¹, Lucia Manangon ^{5,6}, Katherine Vaca ³, Martha Romero-Bastidas ^{7,8}, Henry Pupiales ¹, Verónica Taco ¹ and Patricia Luis ²

¹ Renewable Energy Laboratory, Faculty of Chemical Sciences, Central University of Ecuador, Quito-Ecuador

² Materials & Process Engineering (iMMC-IMAP), UCLouvain, Place Sainte Barbe 2, 1348 Louvain-la-Neuve, Belgium

³ Experimental and Applied Biomedicine Research Group, Health Sciences Faculty, Universidad Particular Internacional SEK (UISEK) Quito 170302, Ecuador

⁴ Food Quality Management, Food Science Department, FARAHA, University of Liège, Belgium

⁵ Institute of Condensed Matter and Nanosciences (IMCN), Université Catholique de Louvain (UCLouvain), Place Louis Pasteur 1, L4.01.09, 1348 Louvain-la-Neuve, Belgium

⁶ Department of Extractive Metallurgy, Escuela Politécnica Nacional, Quito 170517, Ecuador

⁷ Facultad de Ciencias de la Ingeniería e Industrias, Carrera de Alimentos, Centro de Investigación de Alimentos (CIAL), Universidad UTE, Quito 170527, Ecuador

⁸ Dirección de Investigación e Innovación, Instituto Nacional de Patrimonio Cultural (INPC), Quito 170522, Ecuador

* Correspondence: rabahamonde@uce.edu.ec

Abstract

Improving the absorption of visible light in photocatalysts could enhance photocatalytic reactions and reduce energy consumption, particularly in sunny regions like Ecuador. This study reports the synthesis of ZnO and ZnO nanoparticles doped with 1.5 at.% Er, 5 at.% Al, and 1.5 at.% Er:5 at.% Al using the sol-gel method. The effect of doping on the structure, morphology, absorption spectra, and photocatalytic properties was analyzed by XRD, SEM, EDS, and UV-Vis spectrophotometry. XRD confirmed the presence of the wurtzite ZnO structure, and UV-Vis diffuse reflection spectra showed a red-shift in the band-gap for doped ZnO compared to pristine ZnO. Photocatalytic activity was evaluated through the degradation of methyl orange (MO) under artificial visible light and natural sunlight in Quito, Ecuador. ZnO doped with Er/Al nanoparticles exhibited significantly enhanced photocatalytic performance under solar light, suggesting the potential for replacing artificial light and reducing operating costs in photocatalytic processes. Moreover, all doped samples retained the antibacterial properties of ZnO against *B. subtilis*, and Er/Al co-doping improved the inhibition of *E. coli* compared to undoped ZnO.

Keywords: photocatalysis; ZnO nanoparticles; erbium; aluminum; sol-gel; anti-bacterial properties

1. Introduction

The removal of organic pollutants from wastewater is an important measure in environmental protection [1]. Synthetic organic dyes are specifically used in the textile, paper, plastic leather, food, and other industries [2]. Textile wastewater often contains large amount of azo dyes, which are considered as non-biodegradable, persistent and highly stable pollutants in the environment, posing acute hazard to aquatic life [3].

Advanced oxidation processes (AOPs) are considered important, promising, efficient and environmentally friendly methods for the removal of persistent organic pollutants (POPs) such as dyes from water and wastewater [4]. Generally, AOPs rely on the in situ generation of a powerful oxidizing agent, such as hydroxyl radicals ($\bullet\text{OH}$), produced at a sufficient concentration to effectively decontaminate water [5]. In situ formation of $\bullet\text{OH}$ radicals can occur through various chemical, photochemical (heterogeneous photocatalysis), sonochemical or electrochemical reactions. In photochemical processes, heterogeneous photocatalysis involves a process in which a semiconductor (e.g., TiO_2 , ZnO , ZrO_2 , SiO_2 , etc.) is excited by photons from a light source with energy ($h\nu$) greater than or equal to the forbidden energy gap (E_g) of the catalyst, electrons from the valence band (VB) are excited and move to the conduction band (CB) region, leaving holes in the VB. This creates an electron-hole pair (e^-/h^+). The photoexcited electrons then diffuse to the catalyst surface, where they react with adsorbed oxygen, reducing it to a superoxide radical ion ($\text{O}_2^{\bullet-}$). Meanwhile, the holes move towards the surface and react with neighboring adsorbed H_2O or dye molecules, oxidizing them to hydroxyl radicals ($\bullet\text{OH}$) and oxidized dye radical cation ($\text{Dye}^{\bullet+}$) [6]. The most typical catalysts used for photo-electrocatalytic degradation of pollutants are titanium dioxide (TiO_2) and zinc oxide (ZnO) [7,8]. Both are semiconductors with a wide band gap: $E_g = 3.2$ eV for TiO_2 anatase and 3.4 eV for ZnO [9,10]. Titanium dioxide (TiO_2) has been primarily used for decolorizing and decomposing organic dyes [11]. However, ZnO presents a clear advantage compared to TiO_2 under illumination conditions, particularly in inhibiting bacterial growth (even at the lowest tested dose of 10 ppm) [12]. Additionally, ZnO is one of the multifunctional semiconductors with exceptional antibacterial capabilities due to its excellent optical, electrical, mechanical and chemical properties. ZnO typically has a lower cost and high surface-to-volume ratio at the nanometer scale [13]. These characteristics make ZnO a potential alternative that can meet the demand for an efficient and low-cost catalyst, making it a very promising catalyst for the removal of dyes from wastewater [14].

ZnO can be activated under UV irradiation with a wavelength below 387 nm due to its large band gap (3.2-3.4 eV). However, these oxides absorb only a small fraction of sunlight, as less than 5% of solar energy is emitted as UV radiation. This aspect limits the application of these oxides on a large scale [15]. Additionally, the recombination of the photo-generated carrier, hole and electron is also a disadvantage in semiconductor photocatalysis [16]. Developing new photocatalysts by incorporating other elements into ZnO is a major challenge, but it is a promising strategy to enhance the potential application of ZnO -based photocatalysts.

Several dopants are available for ZnO , including anionic, cationic, rare earths elements, co-dopants and couple semiconductors [17]. Cationic doping is typically carried out by the addition of transition metals and elements from group I and group V. The incorporation of dopant cations such as Ce, Mn, Cu, Mg, Al, and others into the crystal lattice of ZnO results in interesting modifications to its properties by introducing additional energy levels to the new photocatalyst [18]. This reduces the activation energy required to initiate photocatalytic activity and increases the catalytic efficiency of the new material. Consequently, cation-doped ZnO exhibits a lower band gap energy compared to undoped ZnO . Additionally, the dopant elements act as electron traps, suppressing the recombination of photogenerated electrons and holes. This process slows down the formation rate of electron-hole pairs. Moreover, dopants can extend the range of light absorption and enhance the photoresponse of cation-doped ZnO in the visible light range [19].

Recently, rare earths such as erbium (Er^{3+}) have been used as dopants, since pristine ZnO cannot directly utilize visible light for photocatalysis due of its wide band gap. Doping rare earths into the ZnO structure can enable the conversion of visible light into ultraviolet light, thereby enhancing the photocatalytic activity of ZnO under visible light. This effect can improve the photocatalytic degradation of dyes in the visible light region, which may be attributed to the enhanced adsorption and 4f electron transition of the rare earth ions [20,21].

Moreover, rare earth metals can reduce the work function of adsorbed oxygen species, increasing the oxygen adsorption capacity and forming more superoxide anions on the ZnO catalyst

surface. This boost in oxidizing species (hydroxyls, peroxy and superoxides) accelerates the rate of photodegradation of organic pollutants [19].

Furthermore, the co-doping of Al/Er in ZnO could further enhance its response to visible light. These doped catalysts may offer an efficient alternative for the degradation of aquatic pollutants under visible light (sunlight), particularly, in countries with high solar incidence, such as Ecuador.

In the present work, ZnO nanoparticles doped with Er³⁺ Al³⁺ were synthesized using the sol-gel method, which is one of the most efficient techniques for nanoparticle synthesis. This method allows precise control over the material's structure during its formation and ensures homogeneity in the solution, resulting in unique properties for the nanoparticles synthesized via the sol-gel method [22]. However, little is known about how co-doping affects the antibacterial properties of the catalyst. The doped ZnO nanoparticles were employed for the removal of dyes in synthetic textile wastewater. The photocatalytic activity was evaluated by degrading methyl orange in water under visible light irradiation and natural sunlight conditions in Quito, Ecuador. The optimal operating conditions were then applied to treat real textile wastewater from a textile company in Quito. Additionally, the effect of the dopant on the antibacterial activity against Gram-positive (*Bacillus subtilis*) and Gram negative (*E. coli*) bacteria was also assessed in this study, shedding light on how doping influences the antimicrobial properties of the catalyst.

2. Experimental Section

2.1. Materials

Zinc nitrate hexahydrate, 99% (metals basis) and erbium nitrate hydrate (99.9%) were purchased from Alfa Aesar (Belgium). Oxalic acid dihydrate (99.5%) and aluminum nitrate nonahydrate (95.5%) were supplied by Sigma Aldrich (Belgium). Ethanol (EtOH, absolute alcohol) was provided by VWR Chemical Co., Ltd. (Belgium). Methyl orange (MO) was obtained from Sigma Aldrich (Fisher Scientific®, Reactive Grade: ACS Certified). All reagents were of analytical grade and used without further purification.

2.2. Synthesis of Catalysts

ZnO was synthesized using the conventional sol-gel method[23]. Specifically, 1.503 g (0.005 mol) of zinc nitrate was dissolved in 30 mL of EtOH and stirred at 60 °C for 30 minutes. Based on Zhang's work [20], the optimal concentrations of the dopants were determined, for this Er(NO₃)₃ and Al(NO₃)₃ with different Er and Al doping amounts (Table 1) were dissolved in this suspension and stirred continuously for 30 minutes to obtain solution A. Solution B was prepared by dissolving 2.507 g (0.02 mol) of oxalic acid dihydrate in 80 mL of EtOH and stirring at 50 °C for 30 minutes. Solution B was then added dropwise to the warm solution A while stirring continuously for 1 hour. A white sol was obtained, which was aged to form a gel and subsequently dried at 80 °C for 24 hours. Finally, ZnO doped and undoped were obtained by thermal treatment at calcination temperature of 400 °C for 1 hour.

Table 1. Composition of catalyst with different dopant ratios.

Sample	at% Er ³⁺	at % Al ³⁺
ZnO	0	0
ZnO-Er	1.5	0
ZnO-Al	0	5
ZnO-Er/Al	1.5	5

2.3. Characterization of Catalyst

The surface morphology of the samples was examined using scanning electron microscopy (SEM) with a JEOL, IT300 instrument, which includes an energy dispersive X-ray (EDX) detector, at accelerating voltages of 15 kV.

The structure of both doped and undoped ZnO powders were analyzed by X-ray diffraction (XRD) using a Bruker AXS - D8 Advance diffractometer with a Cu K α 1 source ($\lambda = 1.5406 \text{ \AA}$). XRD patterns were recorded in the 2θ range from 20° to 80° with a scan rate of 2° min^{-1} and a step of 0.02° .

The average crystallite size was estimated using the Scherrer equation $D = K\lambda/\beta \cos\theta$, where K is a constant (0.92) reflecting the shape factor, $\lambda = 0.154 \text{ nm}$, is the wavelength of CuK α 1 radiation, β is the full width at half maximum (FWHM) of the Bragg peak, and θ is Bragg angle in radians.

Diffuse reflectance UV-Vis (DRUV) spectra were recorded on a Shimadzu UV-Vis-NIR spectrometer (Shimadzu Benelux, The Netherlands) equipped with a Praying Mantis accessory. The spectral range covered was from 200 to 600 nm using the Shimadzu UV software package. A Spectralon pellet was used for background measurement, and the Kubelka–Munk function $F(R)$ was calculated based on the reflectance (R). The band gap energy value (E_g) was calculated from the optical absorption edge in the DRUV spectra using the Tauc method: $(F(R) hv) = A(hv - E_g)^n$, where $F(R)$ is the Kubelka–Munk function, A is a constant, h is Planck's constant, v is the photon frequency, E_g is the optical band gap and n is 2 for a direct semiconductor [18].

Finally, BET surface area was measured using the Micromeritics AutoChem II apparatus.

2.4. Photocatalytic Activity

The photocatalytic activity of pristine ZnO and Er, Al co-doped ZnO was evaluated through the degradation of methyl orange (MO). 0.01, 0.03 and 0.05 g of the photocatalyst were added to 100 mL of MO solution at concentrations of 10, 25 and 50 mg/L in a 200 mL beaker under continuous stirring (Figure 1).

Under artificial visible light, the suspension was irradiated by three different commercial lamps: a 20W UV Blacklight lamp (Sylvania MLX 20W BL368), an 18 W LED lamp (4000K, 2000 lumens, Philips CorePro LED bulb A67 18W 840 Mat), and a 9W LED lamp (4000K, 987 lumens, Osram Parathom Classic A 9W 840 Matt). All lamps were provided by Budgetlight (Belgium) and were positioned 15 cm above the liquid level.

Under solar light, the photocatalytic activity of the catalysts was also studied by degrading aqueous solution of methyl orange at the aforementioned concentrations. The tests were conducted in Quito, Ecuador, during the hours of 11:00 a.m. to 2:00 p.m. to standardize the UV irradiation conditions [24]. Testing was performed when the UV Index in Quito started in 10, according to the Ecuadorian National Institute of Meteorology and Hydrology [25].

During the experiment, 2 mL samples of the solution were collected at various time intervals, centrifuged for 15 minutes at 13000 rpm, and analyzed using a UV-Vis spectrophotometer to determine the concentration of MO at 464 nm. All experiments were conducted in a dark chamber to prevent interference from ambient light and were performed in triplicate, with average values reported.

The removal rate (η) of MO was calculated using the following equations:

$$\eta = \frac{C_0 - C_t}{C_0} \times 100\% \quad (1)$$

$$\eta = \frac{A_0 - A_t}{A_0} \times 100\% \quad (2)$$

where C_0 , and C_t , are the concentrations of MO at $t=0$ and after an irradiation time t , respectively, and, A_0 and A_t are the absorbance of MO at $t=0$ and after an irradiation time t , respectively.

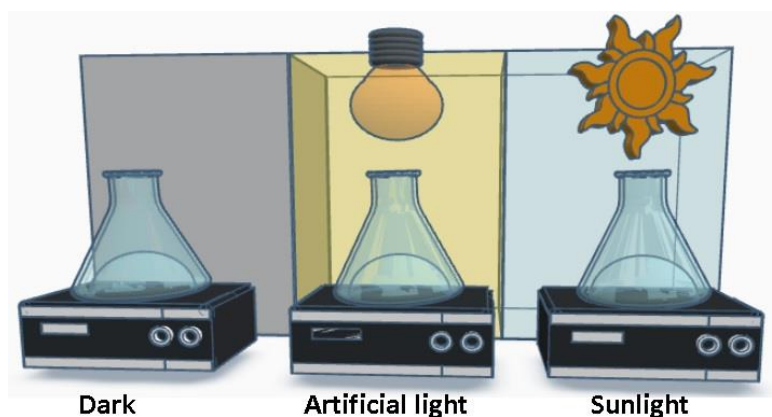


Figure 1. Scheme of experimental determination of photocatalytic activity under different irradiation sources.

2.5. Antibacterial Activity

The antibacterial activity of four catalyst suspensions was evaluated by measuring culture turbidity as an estimation of cell growth in test tubes. The test tubes containing each sample were placed in a thermostatic bath with agitation. Experiments were conducted under both, dark and light conditions to assess the influence of visible light on the antibacterial activity of the synthesized nanoparticles. To simulate dark conditions, the test tubes were wrapped in aluminum foil. For light conditions, an 18 W artificial light bulb (2000 lumens) was positioned 30 cm above the liquid level (Figure 1).

Bacillus subtilis (Gram positive) and *Escherichia coli* (Gram negative) bacteria were used to test the antibacterial activity of nanoparticles. Fresh bacterial suspensions were prepared, with an initial concentration of 10^2 CFU/ mL into the test tubes.

Aqueous catalyst stock suspensions (10 000 mg/L) were prepared under constant stirring. Then, test tubes containing 10 mL of Iso-Sensitest broth medium were supplemented with the appropriate volume of each catalyst's stock suspension to achieve a final catalyst concentration of 300 mg/L. Finally, 100 μ L of bacterial suspension were added to each test tube. Blanks were also prepared for each sample.

To evaluate bacterial growth behavior, the optical density (OD) at 600 nm was measured using a HACH DR1900 UV-vis spectrophotometer. Blank readings were taken to measure the OD due to the culture medium and nanoparticle suspensions. A tube containing only 10 mL of culture medium and 10^2 CFU/ mL of bacteria was used as positive control.

These test tubes were placed in a shaker and were allowed to grow at 35°C overnight, for *B. subtilis* and *E. coli* respectively. The OD at 600 nm of the suspension (containing the bacteria and catalysts) was periodically monitored, and the OD of test tubes after 24 hours was measured. The percentage of growth inhibition compared to the positive control was used as an indicator of the antibacterial activity of the nanoparticles. Cultures of nanoparticle-free medium under the same growth conditions were used as a negative control.

To avoid potential optical interference during optical measurements caused by the light-scattering properties of the nanoparticles, a blank control containing the same culture liquid medium without microorganisms but with the same concentration of nanoparticles was used. After 24 hours, cultures were diluted to 10^{-6} and plated onto tryptic soy agar (TSA) plates in triplicate, then incubated at 37 °C to determine the presence of viable bacteria. Colonies were counted, and the percentage of growth inhibition was calculated and plotted for each catalyst. The experiments were repeated at least three times.

3. Results and Discussion

3.1. Morphology of Composites

The morphology of synthesized pristine ZnO and doped ZnO samples was investigated using SEM. Figure 2 (a-d) shows that Er-Al co-doped ZnO synthesized by the sol-gel method exhibits the typical morphology of ZnO nanoparticles. The pristine ZnO structures in Figure 2a align with the literature, showing a granular form [23]. However, ZnO-Er, ZnO-Al and ZnO-Er/Al nanoparticles displayed a mixed structure of rod-like and flake shapes, with an increased presence of flake shapes when erbium and aluminum were used as dopants (Figure 2b-d). The incorporation of both Er³⁺ and Al³⁺ ions replacing the Zn²⁺ lattice could influence the formation of nano-sized rods.

In addition, the increase in particle size in Er-Al co-doped ZnO suggests that the grain growth of ZnO particles can be hindered by the presence of doping elements (Er and Al) [26]. Moreover, the small size of the particles results in a large specific surface area, leading to strong local aggregation visible in the images. A few larger particles are also observed in the micrograph, which may be due to the aggregation or overlapping of smaller particles [27].

The EDX spectra of ZnO (Figure 2e) was compared with doped ZnO samples (Figure 2f-h), showing the presence of Al, Er and the Al/Er ratio. The weight percentage of oxygen content decreased in co-doped nanopowders, confirming the incorporation of Al and Er into the ZnO matrix. The atomic percentages in all samples were verified and found to be as expected based on the synthesis (Table 2). All doped samples contained only O, Zn, Al, and Er, with no impurity-related peaks observed, indicating the high compositional purity of the samples.

Table 2. Elemental composition of synthesized pristine ZnO and doped ZnO samples.

Sample	at%			
	Zn	O	Er	Al
ZnO	56.61	43.24	0	0
ZnO-Er	50.42	47.32	1.52	0
ZnO-Al	50.10	44.80	0	5.06
ZnO-Er/Al	44.74	48.51	1.46	5.15

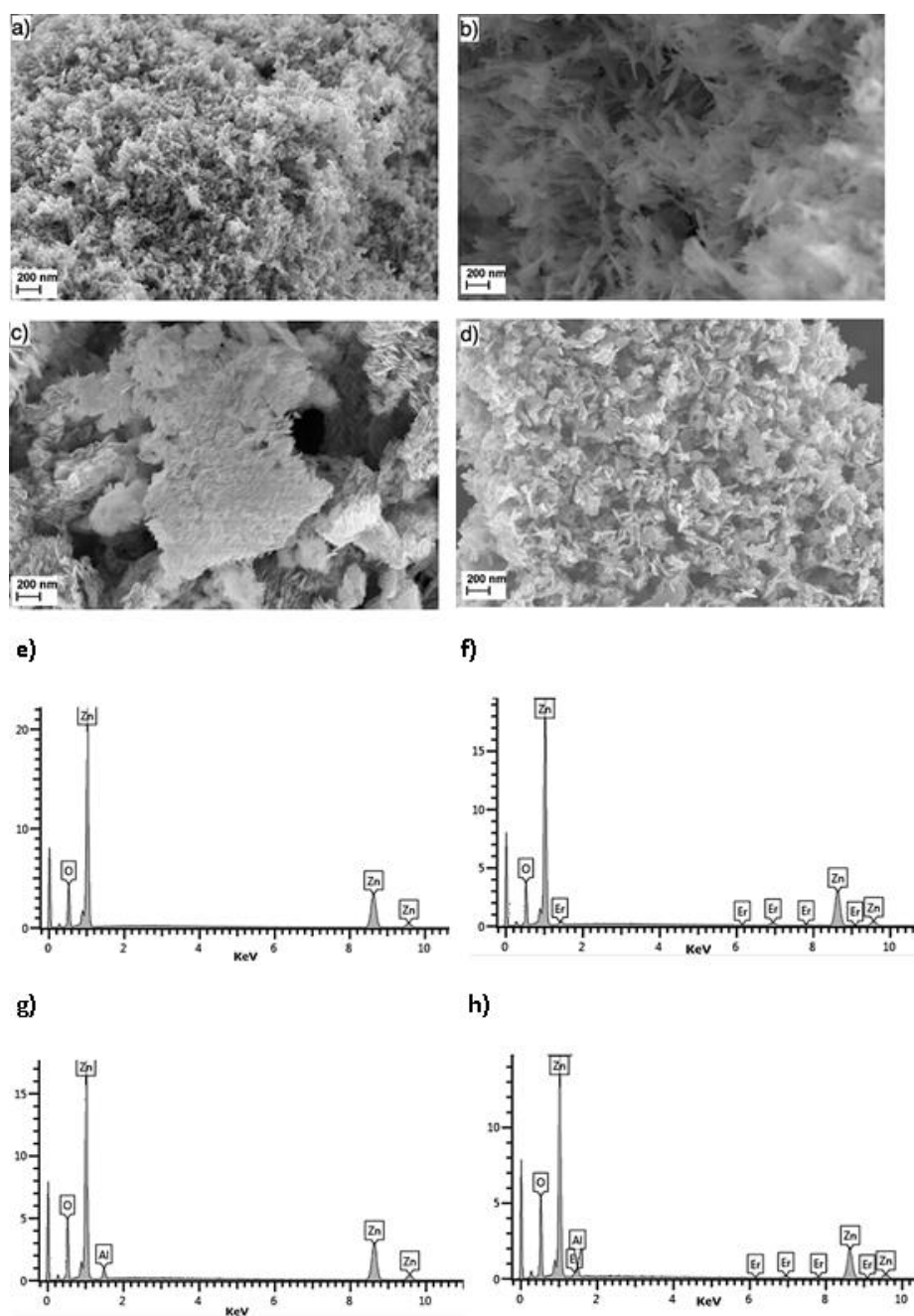


Figure 2. SEM images: **a)** pristine ZnO, **b)** ZnO-Er, **c)** ZnO-Al, and **d)** ZnO-Er/Al, as well as EDX spectrum: **e)** pristine ZnO, **f)** ZnO-Er, **g)** ZnO-Al, and **h)** ZnO-Er/Al. .

3.2. XRD Analysis

The crystal structure of the prepared nanopowders was investigated using powder X-ray diffraction (XRD). Figure 3 displays the XRD patterns of pure ZnO (Figure 3a: ZnO) and doped ZnO samples (Figure 3b: 0% Al, 1,5% Er, Figure 3c: 5% Al, 0% Er and Figure 3d: 5% Al, 1,5% Er). The XRD peaks at 2θ values of 31.8° , 34.4° , 36.3° , 47.6° , 56.6° , 62.9° , 66.5° , 68.0° , 69.1° , and 77.0° were indexed to the (100), (002), (101), (102), (110), (103), (200), (112), (201), and (202) planes of the ZnO crystal, as per the standard data file. These peaks align with the wurtzite type structure, consistent with data from JCPDS card No. 36-1451.

No additional peaks corresponding to any oxides of Al or Er were observed (Figure 3b–d), indicating the complete dissolution of Er and Al dopants within ZnO crystal lattice, where they

occupy Zn sites [28]. Interestingly, the presence of Er and Al caused a decrease in all ZnO peak intensities (Figure 3d), resulting in an increase in the full width at half maximum (FWHM), which implies that Er–Al co-doping inhibited the growth of the crystal size. This suggests that Al³⁺ and Er³⁺ ions substituted Zn²⁺ ions sites within the ZnO crystal, leading to changes in the lattice parameters. Despite these changes, all samples exhibited a preferred orientation along the (101) direction of the ZnO phase.

The calculated crystallite sizes of ZnO-Er, ZnO-Al, ZnO-Er/Al and pristine ZnO were 17.46 nm, 13.90 nm, 10.28 nm, and 21.84 nm, respectively, according to the Scherrer equation [18].

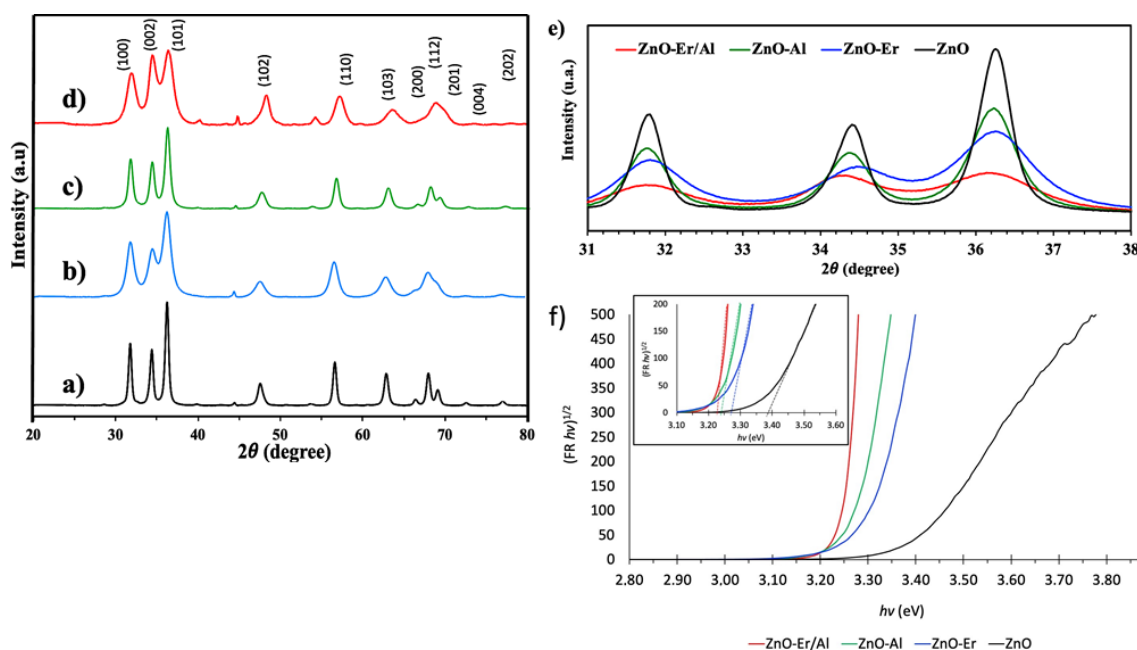


Figure 3. - XRD patterns: **a)** un-doped ZnO, **b)** ZnO-Er, **c)** ZnO-Al and **d)** ZnO-Er/Al and **f)** zoom-in view for the range 31–38°; $(FR\ hv)^{1/2}$ versus $h\nu$ curves for band gap determination of the ZnO and the doped ZnO nanoparticles.

In addition, the ZnO-Er/Al photocatalyst exhibited the highest specific surface area measuring $119.48\text{ m}^2\text{ g}^{-1}$, in comparison to $92.59\text{ m}^2\text{ g}^{-1}$ for pure ZnO. This represents a 22.5% increase in surface area for the ZnO-Er/Al catalyst relative to pure ZnO. The increase in surface area may be attributed to the alteration of the crystal structure of the host ZnO due to the introduction of Er and Al dopants, which likely inhibit crystal growth by integrating these elements into the ZnO lattice. Consequently, the ZnO-Er/Al photocatalyst is more likely to achieve an optimal dye removal rate, owing to its enhanced textural properties.

3.3. Optical Properties

The optical properties of pure and co-doped ZnO nanopowders were analyzed using Diffuse Reflectance Spectroscopy (DRS). The bandgap energy (E_g) was determined using Tauc's plot by applying equation: $(FR\ hv)^{1/2} = A(h\nu - E_g)$ [29]. From the intercept of the linear portion in Figure 3f, the estimated bandgap energies were found to be 3.22 eV for ZnO-Er/Al, 3.23 eV for ZnO-Al, 3.24 eV for ZnO-Er, and 3.32 eV for pure ZnO, as determined by the extrapolation of the $(FR\ hv)^{1/2}$ versus $h\nu$ plots [30].

The data revealed that the co-doping with Er and Al slightly reduced the bandgap energy (E_g) compared to pristine ZnO (Figure 3f). This reduction can be attributed to the defects introduced by the dopants and changes of lattice parameters due to the incorporation of Er and Al into the ZnO crystal lattice. Moreover, these dopants can lead to the formation of oxygen vacancies and additional

energy levels, which increase the average atomic distances and decrease the energy gap [31,32], which can harvest more photons to excite the electron from the valence band [28]. The smallest E_g leads to the highest photocatalytic efficiency under visible light illumination [31,33], which correspond to the sample co-doped with both Er and Al.

3.4. Catalyst Dosage on Metil Orange Degradation

To determine the optimal catalyst concentration for methyl orange (MO) degradation, experiments were conducted using three different concentrations of ZnO-Er/Al: 0.01%, 0.03, 0.05% wt under an 18W LED lamp with 25 mg /L MO solutions. The results indicated MO removal efficiencies 85.8%, 98.7%, and 97.5 % for the 0.01%, 0.03%, and 0.05% wt concentrations, respectively.

This trend suggest that increasing the photocatalyst concentration leads to a higher number of active sites on the catalyst surface, thereby enhancing the formation of reactive radicals and increasing the degradation efficiency of MO [23]. However, there is a slightly higher value for the 0.03 %wt (0.3g/L) concentration compared to the following concentration 0.05 %wt (0.5g/L), which could be due to the probability that at higher catalyst concentration the probability of aggregation of catalyst molecules also increases, decreasing the amount of available active sites where photocatalysis takes place. Thus, 0.3g/L (0.03%wt) of catalyst was chosen as the optimal amount to continue the study.

3.5. Photocatalytic Performance of Synthesized Nanoparticles

Following a comparison of various light sources (see supporting information S1), it was concluded that there were no significant differences in photocatalytic performance across the different lamps. Therefore, only the results obtained using the 18W LED lamp are presented here, due to its lower energy consumption compared to the other light sources tested.

Since the photocatalytic reaction occurs on the catalyst surface, and the recombination of photogenerated electron-hole pairs happens within nanosecond, efficient charge transfer to reactants is possible only when the electron donor or acceptor is pre-adsorbed on the catalyst surface before the reaction begins [34]. To account for this, adsorption equilibrium of MO was studied. Suspensions of the catalyst were stirred in the dark for 30 minutes to ensure MO adsorption on the oxide surfaces had reached equilibrium. The amount of MO adsorbed on each oxide was determined by comparing the concentration before and after stirring.

Preliminary adsorption of substrates is critical factor for achieving high degradation efficiency. As summarized in Figure 4a, the adsorption capacity of the capacity of the catalysts followed the order: ZnO-Er/Al > ZnO-Al > ZnO-Er > ZnO. ZnO exhibited the lowest adsorption capacity for MO, while ZnO-Er/Al had the highest. All doped ZnO samples demonstrated stronger adsorption capacities than pure ZnO, suggesting that higher reactivity is likely in samples with stronger adsorption capacities. This data shows a clear positive correlation between photocatalytic activity and the amount of substrate adsorbed on the catalysts surface, indicating that adsorption plays a vital role in determining photocatalytic activity.

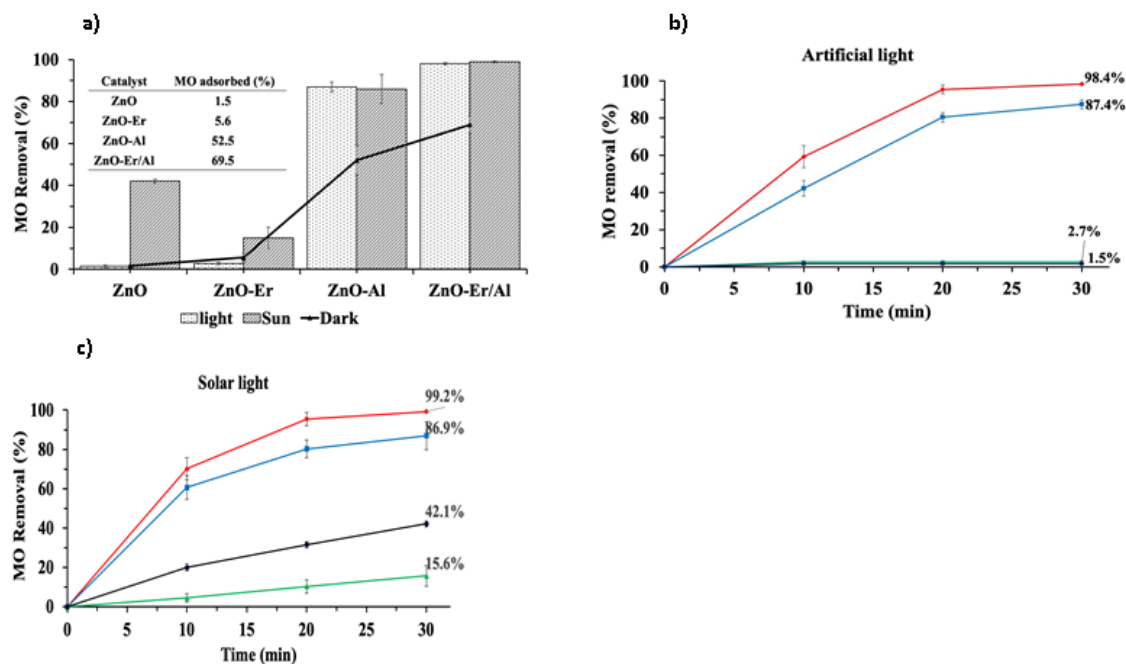
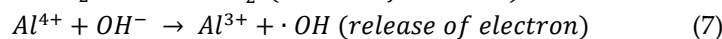
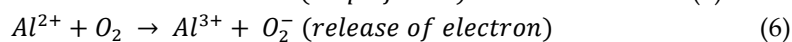
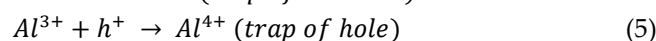
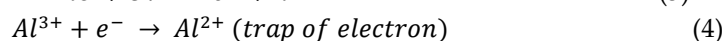
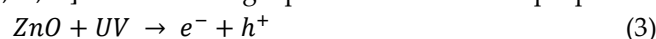


Figure 4. Photocatalytic degradation curves of methyl orange (25 mg/L) using ZnO, ZnO-Er, ZnO-Al, and ZnO-Er/Al catalysts. **a)** Comparison of the photodegradation rate of MO using different catalysts after 30 minutes of exposure, **b)** under artificial white light irradiation (18W) and **c)** under solar light irradiation.

Additionally, ZnO co-doped with Er and Al exhibited a significantly enhanced removal efficiency, followed by ZnO doped solely with Al. In this study, the Al^{3+} ions act as electron and hole traps, effectively preventing recombination and thereby improving photocatalytic activity [22,35]. This enhancement is attributed to the presence of Al^{3+} on the catalyst surface, which, by being placed at the donor level, inhibits the recombination of excited electrons and holes within the valance band. Furthermore, Al doping leads to a reduction in band gap energy (as discussed in section 3.3), creating a sideways band that forms an intermediate energy level between the conduction and valence bands. This reduced bandgap facilitates more efficient photocatalysis by reducing the energy barrier for electron excitation [22,36,37]. The following equations describe the proposed mechanism:



As illustrated in Equations (4) and (5), Al^{3+} ions can react with electron and holes, resulting in the formation of Al^{2+} and Al^{4+} ions. These ions are less stable compared to Al^{3+} and react with oxygen and hydroxyl ion on the catalyst surface to achieve stability, generating superoxide and hydroxyl radicals [22]. Consequently, Al^{3+} ions capture electrons and holes, preventing recombination, and release them at the catalyst surface (Equations (6) and (7)).

Moreover, Er doping in ZnO-Al facilitated visible-to-UV up-conversion, which enhanced the photocatalytic oxidation of MO. This is due to Er^{3+} 's ability to accommodate discrete 4f energy levels of rare-earths ions within ZnO's broad forbidden bandgap, thereby tuning excitation and emission wavelengths [38]. Although Er^{3+} has efficient luminescence in the green spectrum and low UV absorption, its doping with ZnO enhances both absorption and luminescence efficiency. Additionally, Er doping reduces the crystal size of ZnO, leading to an overall improvement in photocatalytic activity [26]. As a result, ZnO-Er/Al presents a promising class of luminescent materials.

Interestingly, the Er-doped ZnO exhibited lower photocatalytic activity under artificial light (Figure 4b). This result may stem from the fact that the band-gap energies of the rare-earth oxides

used in these experiments were insufficient to initiate a photocatalytic reaction after UV irradiation [34,38]. In contrast, ZnO-Er showed a slight improvement in photocatalytic activity under sunlight (Figure 4c), which may be attributed to the high level of UV radiation in Quito, Ecuador, during the evaluation period. This observation is further supported by increase in pure ZnO's photocatalytic activity in under sunlight as well.

3.6. Determination of Antibacterial Activity of Doped and Undoped ZnO Samples

The catalyst concentration of 0.03%wt was found to be an effective minimum inhibitory concentration (MIC) against *Bacillus subtilis* and *Escherichia coli* under both dark and light conditions, as illustrated in Figure 5.

For *B. subtilis*, all catalysts exhibited remarkable bacterial growth inhibition (~ 93%). Notably, the dopants had no adverse effect on the inhibition of *B. subtilis* growth, as shown in Figure 5a. In the case of *E. coli*, the undoped ZnO displayed a lower inhibitory activity (78%) compared of the doped samples. Doping appeared to enhance the inhibitory effects, with the ZnO-Er/Al sample demonstrating the highest antibacterial activity (94%) among the doped samples (Figure 5b).

ZnO is known to act as a photocatalyst under UV light, which could lead to the production of reactive oxygen species (ROS). However, the antibacterial tests conducted in this study also yielded positive results under dark conditions. These findings indicate that ZnO retains its antibacterial properties even in the absence of light, consistent with previous studies [39].

The antibacterial activity of ZnO nanoparticles against Gram-positive and Gram-negative bacteria may be attributed to their ability to generate reactive oxygen species (ROS) and to coordination bonds between metal ions and the nitrogen, oxygen, or sulfur atoms presents in biomolecules [40,41]. The enhanced inhibition of *B. subtilis* could be due to the greater ability of Zn²⁺ ions to penetrate and damage the cell walls of Gram-positive bacteria, which tend to be softer than those of Gram-negative bacteria such as *E. coli*. Although the exact reason for zinc's different affinity towards Gram-positive bacteria remains unclear, it could be related to differences in the protein composition of their cell walls [42].

ROS facilitate mass transport, and the dispersion of reactant molecules generated by mitochondria. These species can damage cellular DNA and proteins either direct by diffusion or through endocytic vesicle formation. When particles are incorporated into the cytoplasm or nucleus, they can disrupt the plasma membrane or DNA [43]. Additionally, doping ZnO nanoparticles with ions may enhance their antibacterial activity. Saxena & Pandey (2019) demonstrated that Al-doped ZnO nanoparticles showed superior antibacterial activity against *E. coli* and *E. hirae* compared to undoped ZnO, likely due to electrostatic interactions between bacterial cell and positively charged Al-doped nanoparticles [44]. Similarly, studies have found that lanthanide oxides nanoparticles, including Er oxide, are effective against *E. coli* and *Pseudomonas aeruginosa* under both dark and light conditions [45].

In this study, Er and Al co-doping of ZnO significantly increased antibacterial activity against *E. coli* compared to undoped ZnO. Furthermore, the co-doping did not negatively affect the high antibacterial efficacy exhibited by pure ZnO against *B. subtilis*.

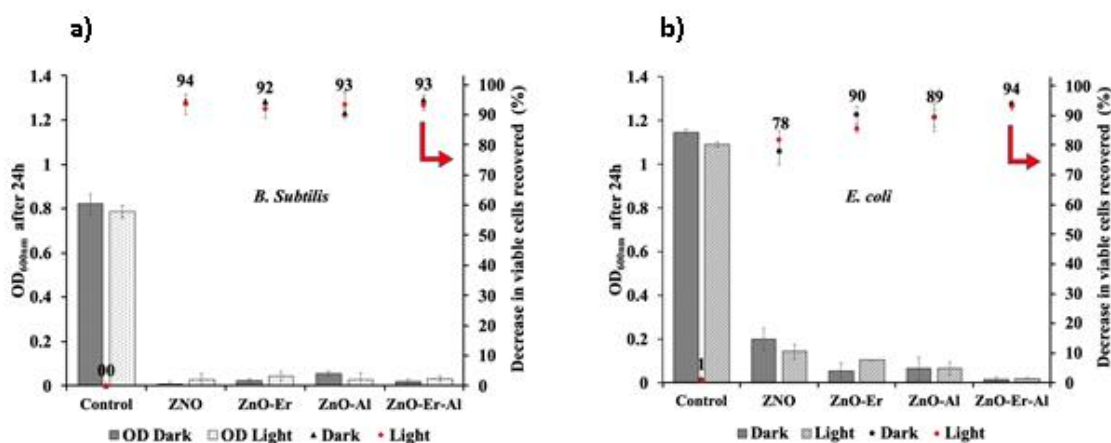


Figure 5. Effect of dopant on ZnO nanoparticles in inhibiting the growth of (a) *B. subtilis* and (b) *E. coli* strains. Growth was analyzed by measuring optical density (OD) at 600 nm after 24 hours, and inhibition was determined by counting viable bacteria recovered from TSA plates following 24 hours of incubation at 37°C.

4. Conclusions

The ZnO-Er/Al photocatalyst, synthesized via the sol-gel method, demonstrated a simple and flexible preparation process with high photocatalytic efficiency. SEM-EDX analysis confirmed successful incorporation of Er and Al ions into the ZnO structure. While Er doping slightly decreased photocatalytic activity, Al doping significantly enhanced it, and co-doping with Er and Al yielded the highest methyl orange (MO) degradation efficiency. Both artificial and natural sunlight exhibited comparable effectiveness in MO degradation, with sunlight showing a slight improvement. This enhancement is attributed to the broader absorption spectrum of the doped catalyst, slightly shifted towards the visible region, resulting in a reduced band gap. These results suggest that sunlight could replace artificial light for MO degradation, thereby reducing operational costs of the ZnO-Er/Al catalyst.

In terms of antibacterial activity, co-doping with Er and Al enhanced the inhibition of *E. coli* compared to pure ZnO, while maintaining the strong antibacterial properties of ZnO against *B. subtilis*. These findings highlight the promising potential of ZnO-Er/Al catalysts for both environmental remediation and antimicrobial applications.

Acknowledgments: The authors acknowledge the support provided by L Académie de Recherche et d'Enseignement Supérieur (ARES) and Central University of Ecuador for financially supporting this work (RFCQ-CQ-SO13-186-2017), and Project 69 condolatory 2018 UCE. The authors greatly thank Frédéric Van Wonterghem and Laurence Ryelandt from pole Materials and Processes Engineering (IMAP) UCLouvain, for the SEM and EDX measurements. Finally, the authors thank Eric Gaigneaux and National Foundation for Scientific Research (FNRS-FRS, Belgium) for UV-VIS DRS.

References

1. N. Singhal, S. Selvaraj, Y. Sivalingam, G. Venugopal, Study of photocatalytic degradation efficiency of rGO/ZnO nano-photocatalyst and their performance analysis using scanning Kelvin probe, *J. Environ. Chem. Eng.* 10 (2022) 107293. <https://doi.org/10.1016/j.jece.2022.107293>.
2. S. Anandan, V. Kumar Ponnusamy, M. Ashokkumar, A review on hybrid techniques for the degradation of organic pollutants in aqueous environment, *Ultrason. Sonochem.* 67 (2020). <https://doi.org/10.1016/j.ultsonch.2020.105130>.
3. H. Zhu, R. Jiang, Y. Fu, Y. Guan, J. Yao, L. Xiao, G. Zeng, Effective photocatalytic decolorization of methyl orange utilizing TiO₂/ZnO/chitosan nanocomposite films under simulated solar irradiation, *Desalination*. 286 (2012) 41–48. <https://doi.org/10.1016/j.desal.2011.10.036>.

4. Z. Mirzaeifard, Z. Shariatinia, M. Jourshabani, S.M. Rezaei Darvishi, ZnO Photocatalyst Revisited: Effective Photocatalytic Degradation of Emerging Contaminants Using S-Doped ZnO Nanoparticles under Visible Light Radiation, *Ind. Eng. Chem. Res.* 59 (2020) 15894–15911. <https://doi.org/10.1021/acs.iecr.0c03192>.
5. M.A. Oturan, J.J. Aaron, Advanced oxidation processes in water/wastewater treatment: Principles and applications. A review, *Crit. Rev. Environ. Sci. Technol.* 44 (2014) 2577–2641. <https://doi.org/10.1080/10643389.2013.829765>.
6. G.K. Weldegebrerial, Synthesis method, antibacterial and photocatalytic activity of ZnO nanoparticles for azo dyes in wastewater treatment: A review, *Inorg. Chem. Commun.* 120 (2020). <https://doi.org/10.1016/j.inoche.2020.108140>.
7. L. Pan, G.Q. Shen, J.W. Zhang, X.C. Wei, L. Wang, J.J. Zou, X. Zhang, TiO₂-ZnO Composite Sphere Decorated with ZnO Clusters for Effective Charge Isolation in Photocatalysis, *Ind. Eng. Chem. Res.* 54 (2015) 7226–7232. <https://doi.org/10.1021/acs.iecr.5b01471>.
8. A.H. Zyoud, A. Zubi, S. Hejjawi, S.H. Zyoud, M.H. Helal, S.H. Zyoud, N. Qamhieh, A.R. Hajamohideen, H.S. Hilal, Removal of acetaminophen from water by simulated solar light photodegradation with ZnO and TiO₂ nanoparticles: Catalytic efficiency assessment for future prospects, *J. Environ. Chem. Eng.* 8 (2020) 104038. <https://doi.org/10.1016/j.jece.2020.104038>.
9. D. Tekin, H. Kiziltas, H. Ungan, Kinetic evaluation of ZnO/TiO₂ thin film photocatalyst in photocatalytic degradation of Orange G, *J. Mol. Liq.* 306 (2020). <https://doi.org/10.1016/j.molliq.2020.112905>.
10. E.S. Araújo, B.P. Da Costa, R.A.P. Oliveira, J. Libardi, P.M. Faia, H.P. De Oliveira, TiO₂/ZnO hierarchical heteronanostructures: Synthesis, characterization and application as photocatalysts, *J. Environ. Chem. Eng.* 4 (2016) 2820–2829. <https://doi.org/10.1016/j.jece.2016.05.021>.
11. K. Rajeshwar, M.E. Osugi, W. Chanmanee, C.R. Chenthamarakshan, M.V.B. Zanoni, P. Kajitvichyanukul, R. Krishnan-Ayer, Heterogeneous photocatalytic treatment of organic dyes in air and aqueous media, *J. Photochem. Photobiol. C Photochem. Rev.* 9 (2008) 171–192. <https://doi.org/10.1016/j.jphotochemrev.2008.09.001>.
12. L.K. Adams, D.Y. Lyon, P.J.J. Alvarez, Comparative eco-toxicity of nanoscale TiO₂, SiO₂, and ZnO water suspensions, *Water Res.* 40 (2006) 3527–3532. <https://doi.org/10.1016/j.watres.2006.08.004>.
13. S. Balta, A. Sotto, P. Luis, L. Benea, B. Van der Bruggen, J. Kim, A new outlook on membrane enhancement with nanoparticles: The alternative of ZnO, *J. Memb. Sci.* 389 (2012) 155–161. <https://doi.org/10.1016/j.memsci.2011.10.025>.
14. J. Yoon, S.-G. Oh, Synthesis of amine modified ZnO nanoparticles and their photocatalytic activities in micellar solutions under UV irradiation, *J. Ind. Eng. Chem.* 96 (2021) 390–396. <https://doi.org/10.1016/j.jiec.2021.01.043>.
15. R. Dagher, P. Drogui, D. Robert, Modified TiO₂ for environmental photocatalytic applications: A review, *Ind. Eng. Chem. Res.* 52 (2013) 3581–3599. <https://doi.org/10.1021/ie303468t>.
16. C. Gomez-Solís, J.C. Ballesteros, L.M. Torres-Martínez, I. Juárez-Ramírez, L.A. Díaz Torres, M. Elvira Zarazua-Morin, S.W. Lee, Rapid synthesis of ZnO nano-corncoobs from Nital solution and its application in the photodegradation of methyl orange, *J. Photochem. Photobiol. A Chem.* 298 (2015) 49–54. <https://doi.org/10.1016/j.jphotochem.2014.10.012>.
17. I. Ahmad, S. Shukrullah, M.Y. Naz, H.N. Bhatti, M. Ahmad, E. Ahmed, S. Ullah, M. Hussien, Recent Progress in Rare Earth Oxides and Carbonaceous Materials Modified ZnO Heterogeneous Photocatalysts for Environmental and Energy Applications, *J. Environ. Chem. Eng.* 10 (2022) 107762. <https://doi.org/10.1016/j.jece.2022.107762>.
18. J. de L. Andrade, A.G. Oliveira, V.V.G. Mariucci, A.C. Bento, M.V. Companhoni, C.V. Nakamura, S.M. Lima, L.H. da C. Andrade, J.C.G. Moraes, A.A.W. Hechenleitner, E.A.G. Pineda, D.M.F. de Oliveira, Effects of Al³⁺ concentration on the optical, structural, photocatalytic and cytotoxic properties of Al-doped ZnO, *J. Alloys Compd.* 729 (2017) 978–987. <https://doi.org/10.1016/j.jallcom.2017.09.128>.
19. K.M. Lee, C.W. Lai, K.S. Ngai, J.C. Juan, Recent developments of zinc oxide based photocatalyst in water treatment technology: A review., *Water Res.* 88 (2016) 428–448. <https://doi.org/10.1016/j.watres.2015.09.045>.

20. X. Zhang, S. Dong, X. Zhou, L. Yan, G. Chen, D. Zhou, A facile one-pot synthesis of Er-Al co-doped ZnO nanoparticles with enhanced photocatalytic performance under visible light, *Mater. Lett.* 143 (2015) 312–314. <https://doi.org/10.1016/j.matlet.2014.12.094>.
21. M. Prathap Kumar, G.A. Suganya Josephine, G. Tamilarasan, A. Sivasamy, J. Sridevi, Rare earth doped semiconductor nanomaterials and its photocatalytic and antimicrobial activities, *J. Environ. Chem. Eng.* 6 (2018) 3907–3917. <https://doi.org/10.1016/j.jece.2018.05.046>.
22. R. Mahdavi, S.S.A. Talesh, Sol-gel synthesis, structural and enhanced photocatalytic performance of Al doped ZnO nanoparticles, 28 (2017) 1418–1425.
23. X. Chen, Z. Wu, D. Liu, Z. Gao, Preparation of ZnO Photocatalyst for the Efficient and Rapid Photocatalytic Degradation of Azo Dyes, *Nanoscale Res. Lett.* 12 (2017) 4–13. <https://doi.org/10.1186/s11671-017-1904-4>.
24. D. Rajamanickam, M. Shanthi, Photocatalytic degradation of an organic pollutant, 4-nitrophenol by zinc oxide - UV process, *Res. J. Chem. Environ.* 9 (2012) S1858–S1868.
25. Ambient secretary government of Quito Ecuador, Ambient secretary government of Quito Ecuador, (2020).
26. N.K. Divya, P.P. Pradyumnan, Solid state synthesis of erbium doped ZnO with excellent photocatalytic activity and enhanced visible light emission, *Mater. Sci. Semicond. Process.* 41 (2016) 428–435.
27. M. Bououdina, S. Azzaza, R. Ghomri, M.N. Shaikh, J.H. Dai, Y. Song, W. Song, W. Cai, M. Ghers, Structural and magnetic properties and DFT analysis of ZnO:(Al,Er) nanoparticles, *RSC Adv.* 7 (2017) 32931–32941. <https://doi.org/10.1039/c7ra01015j>.
28. R. Ghomri, M.N. Shaikh, M.I. Ahmed, W. Song, W. Cai, M. Bououdina, M. Ghers, Pure and (Er, Al) co-doped ZnO nanoparticles: synthesis, characterization, magnetic and photocatalytic properties, *J. Mater. Sci. Mater. Electron.* 29 (2018) 10677–10685. <https://doi.org/10.1007/s10854-018-9136-7>.
29. P. Makuła, M. Pacia, W. Macyk, How To Correctly Determine the Band Gap Energy of Modified Semiconductor Photocatalysts Based on UV-Vis Spectra, *J. Phys. Chem. Lett.* 9 (2018) 6814–6817. <https://doi.org/10.1021/acs.jpcclett.8b02892>.
30. B.D. Viezbicke, S. Patel, B.E. Davis, D.P. Birnie, Evaluation of the Tauc method for optical absorption edge determination: ZnO thin films as a model system, *Phys. Status Solidi Basic Res.* 252 (2015) 1700–1710. <https://doi.org/10.1002/pssb.201552007>.
31. S.G. Ullattil, P. Periyat, B. Naufal, M.A. Lazar, Self-Doped ZnO Microrods - High Temperature Stable Oxygen Deficient Platforms for Solar Photocatalysis, *Ind. Eng. Chem. Res.* 55 (2016) 6413–6421. <https://doi.org/10.1021/acs.iecr.6b01030>.
32. M.R.A. Kumar, C.R. Ravikumar, H.P. Nagaswarupa, B. Purshotam, B.A. Gonfa, H.C.A. Murthy, F.K. Sabir, S. Tadesse, Evaluation of bi-functional applications of ZnO nanoparticles prepared by green and chemical methods, *J. Environ. Chem. Eng.* 7 (2019) 103468. <https://doi.org/10.1016/j.jece.2019.103468>.
33. X. Zhang, Y. Chen, S. Zhang, C. Qiu, High photocatalytic performance of high concentration Al-doped ZnO nanoparticles, *Sep. Purif. Technol.* 172 (2017) 236–241. <https://doi.org/10.1016/j.seppur.2016.08.016>.
34. A.W. Xu, Y. Gao, H.Q. Liu, The preparation, characterization, and their photocatalytic activities of rare-earth-doped TiO₂ nanoparticles, *J. Catal.* 207 (2002) 151–157. <https://doi.org/10.1006/jcat.2002.3539>.
35. S. Tao, M. Yang, H. Chen, S. Zhao, G. Chen, Continuous Synthesis of Ag/AgCl/ZnO Composites Using Flow Chemistry and Photocatalytic Application, *Ind. Eng. Chem. Res.* 57 (2018) 3263–3273. <https://doi.org/10.1021/acs.iecr.7b05263>.
36. M. Fu, Y. Li, S. Wu, P. Lu, J. Liu, F. Dong, Sol-gel preparation and enhanced photocatalytic performance of Cu-doped ZnO nanoparticles, *Appl. Surf. Sci.* 258 (2011) 1587–1591. <https://doi.org/10.1016/j.apsusc.2011.10.003>.
37. S. Dong, K. Xu, J. Liu, H. Cui, Photocatalytic performance of ZnO:Fe array films under sunlight irradiation, *Phys. B Condens. Matter.* 406 (2011) 3609–3612. <https://doi.org/10.1016/j.physb.2011.06.053>.
38. A. Layek, S. Banerjee, B. Manna, A. Chowdhury, Synthesis of rare-earth doped ZnO nanorods and their defect-dopant correlated enhanced visible-orange luminescence, *RSC Adv.* 6 (2016) 35892–35900. <https://doi.org/10.1039/c6ra02278b>.
39. L. Zhang, Y. Jiang, Y. Ding, M. Povey, D. York, Investigation into the antibacterial behaviour of suspensions of ZnO nanoparticles (ZnO nanofluids), *J. Nanoparticle Res.* 9 (2007) 479–489. <https://doi.org/10.1007/s11051-006-9150-1>.

40. K.R. Raghupathi, R.T. Koodali, A.C. Manna, Size-dependent bacterial growth inhibition and mechanism of antibacterial activity of zinc oxide nanoparticles, *Langmuir*. 27 (2011) 4020–4028. <https://doi.org/10.1021/la104825u>.
41. A. Prasert, S. Sontikaew, D. Sriprapai, S. Chuangchote, Polypropylene/ZnO Nanocomposites: Mechanical Properties, Photocatalytic Dye Degradation, and Antibacterial Property, *Materials (Basel)*. 13 (2020) 914. <https://doi.org/10.3390/ma13040914>.
42. R. Bahamonde Soria, J. Zhu, I. Gonza, B. Van der Bruggen, P. Luis, Effect of (TiO₂: ZnO) ratio on the anti-fouling properties of bio-inspired nanofiltration membranes, *Sep. Purif. Technol.* 251 (2020). <https://doi.org/10.1016/j.seppur.2020.117280>.
43. T. Munawar, S. Yasmeen, F. Mukhtar, M.S. Nadeem, K. Mahmood, M. Saqib Saif, M. Hasan, A. Ali, F. Hussain, F. Iqbal, Zn_{0.9}Ce_{0.05}M_{0.05}O (M = Er, Y, V) nanocrystals: Structural and energy bandgap engineering of ZnO for enhancing photocatalytic and antibacterial activity, *Ceram. Int.* 46 (2020) 14369–14383. <https://doi.org/10.1016/j.ceramint.2020.02.232>.
44. V. Saxena, L.M. Pandey, Synthesis, characterization and antibacterial activity of aluminum doped zinc oxide, *Mater. Today Proc.* 18 (2019) 1388–1400. <https://doi.org/10.1016/j.matpr.2019.06.605>.
45. K. Dědková, Kuzníková, L. Pavelek, K. Matějová, J. Kupková, K. Čech Barabaszová, R. Váňa, J. Burda, J. Vlček, D. Cvejn, J. Kukutschová, Daylight induced antibacterial activity of gadolinium oxide, samarium oxide and erbium oxide nanoparticles and their aquatic toxicity, *Mater. Chem. Phys.* 197 (2017) 226–235. <https://doi.org/10.1016/j.matchemphys.2017.05.039>.

Disclaimer/Publisher's Note: The statements, opinions and data contained in all publications are solely those of the individual author(s) and contributor(s) and not of MDPI and/or the editor(s). MDPI and/or the editor(s) disclaim responsibility for any injury to people or property resulting from any ideas, methods, instructions or products referred to in the content.